ARTICLE

Lubricated Tribology of a Eutectic Aluminium-Silicon Alloy in the Ultra-Mild Wear and Mild Wear Regimes for Long Sliding Times

Anirban Mahato, Anil Sachdev, and S. K. Biswas*

Mechanical Engineering Department, Indian Institute of Science, Bangalore 560012, India, and Chemical Sciences and Materials Systems Lab, General Motors Research and Development Centre, Warren, Michigan

ABSTRACT Aluminium-silicon alloy, an important material used for the construction of internal combustion engines, exhibit pressure induced distinct regimes of wear and friction; ultra-mild and mild. In this work the alloy is slid lubricated against a spherical steel pin at contact pressures characteristic of the two test regimes, at a very low sliding velocity. In both cases, the friction is controlled at the initial stages of sliding by the abrasion of the steel pin by the protruding silicon particles of the disc. The generation of nascent steel chips helps to breakdown the additive in the oil by a cationic exchange that yields chemical products of benefits to the tribology. The friction is initially controlled by abrasion, but the chemical products gain increasing importance in controlling friction with sliding time. After long times, depending on contact pressure, the chemical products determine sliding friction exclusively. In this paper, a host of mechanical and spectroscopic techniques are used to identify and characterize mechanical damage and chemical changes. Although the basic dissipation mechanisms are the same in the two regimes, the matrix remains practically unworn in the low-pressure ultra-mild wear regime. In the higher pressure regime at long sliding times a small but finite wear rate prevails. Incipient plasticity in the subsurface controls the mechanism of wear.

KEYWORDS: aluminium−silicon alloy • ultra-mild wear • mild wear • tribofilm • time-dependent transition

1. INTRODUCTION

Aluminum alloys provide an attractive option for use as an engine material in internal combustion engines because of their good power to weight ratio. Challenges with aluminum, compared with iron are its lower strength at high temperatures and adhesion to steel counterfaces, both of which affect wear resistance. Aluminum alloys, if not designed properly, show damage at the top dead centre of an engine stroke where the stresses are high and boundary lubrication conditions may prevail.

One of the mitigating measures to counter the concern of poorer wear resistance is to introduce a hard second phase, generally silicon, into the alloy. A two-stage honing process releases the silicon particle by chemical or mechanical action (1−3) to stand proud of the surface. It has also been shown, using the Greenwood and Tripp model, that the roughness imparted by honing reduces the peak contact pressure (3), which discourages plastic deformation of the matrix alloy. The particles bear the load and provide scuffing and wear resistance during use. When the bore surface microstructure and properties are poorly designed, the Si particles can wear and fracture by abrasion during sliding and can sink into the matrix (4, 5). As the height of the silicon protrusion reduces with sliding, the matrix alloy is exposed to direct metal-to-metal contact with the counterface asperities. The longevity of these silicon protrusions depend on sliding time and applied normal load (6, 7). For relatively short sliding times it has been shown (6) that the wear rate is practically zero when the contact pressure is low. This stage is designated as the ultra-mild wear (UMW) stage. Metal-to-metal contact, however, occurs rapidly at high contact pressures, and the wear rate is high under these conditions. This stage is designated mild wear (MW).

Another mitigating measure related to aluminum wear is to use an oil-based lubricant which contains zinc and/or molybdenum based additives (8, 9), which is used when the substrate and the counterface are both iron-based alloys. The additives under traction decompose and sometimes recombine to yield a variety of products at the interface that provide load support, wear resistance, and low dissipation (8−10). The products are well-identified and the chemical processes are well-understood. However, when the wear surface is an aluminium−silicon alloy, the protection these products provide is not conclusively established.

When the contact pressures are low in the ultra-mild wear regime, the silicon particles support the load. When the particles disappear with sliding time or at higher pressures, a tribofilm, which comes into existence because of the interaction of the substrate with the decomposed components of the additives and the ultra fine aluminium grains, bears the load (11). Some workers (12−14) contend that zinc-dialkyl-dithiophosphates (ZDDP) antiwear pads form on top of the silicon particles. Although Das et al. (15) did not

* Corresponding author. Phone: +918022932589. Fax: +918023600648. E-mail: skbis@mecheng.iisc.ernet.in.

Received for review June 24, 2010 and accepted September 13, 2010

DOI: 10.1021/am100550m

Published on Web 09/23/2010

detect a general decomposition of ZDTP (Zinc-dialkyl-thiophosphate) at the Fe−Al/Si interface, they detected phosphorus on the protruding silicon surface and attributed low friction in boundary lubrication to the decomposition of the additive to various glassy phosphates. Others (1) have challenged these findings as they find the tribofilm to be principally made up of aluminium alloy wear particles. There is some evidence (16, 17) that suggests that the boundary lubrication mechanism for Fe/Al interaction is not dictated by chemical reaction but by adsorption of the additives (18, 19), except in the case of chlorine-based additives. This hypothesis has been demonstrated for fatty acids (18, 20, 21) and ZDDP (22, 23). The adsorbed molecule prevents the reduction of the aluminium oxide to aluminium metal. This has also been demonstrated for an amine salt of an acid phosphate. There is, however, a lack of unanimity amongst research workers regarding the role of ZDDP in the tribology of systems where one of the matrix surfaces is aluminium. Wan et al. (24) report that at low concentration of 1%, that ZDTP has no effect on Fe/Al boundary lubrication tribology. At higher concentrations, $AlPO_4$ formed at the interface impairs wear resistance. However, earlier work (22) has suggested that ZDTP polymerizes at the interface and provides wear protection. The varied interpretations described above suggest that such a protective role cannot be taken for granted.

The pressure dependence of quantitative and qualitative changes in tribology of aluminium−silicon alloy has been demonstrated in dry sliding for short runs (6). The lubricated tribology of these alloys over prolonged sliding poses additional questions: Does lubrication protect the protruding silicon by forming a tribofilm? If not, does silicon wear with time? If so, then does the matrix alloy become involved in the tribology at the interface? How does this tribology evolve with time and do the lubricant additives provide protection? Does this chemical interaction depend on contact pressure? Given this transient nature of lubricated tribology of aluminium−silicon alloys, what is the timeframe to obtain steady state? Ideally speaking, the experiments need to be done for a practical length of time of relevance to the regrinding of the engine bore. We have, however, found in this work that both the friction coefficient and the wear rate vary with time, albeit under the ideal test conditions used here, in the first 10−15 h. After this time, the tribological characteristic are more or less invariant with time. We have thus run the experiments for 40 h.

This report looks at long term lubricated tribology of aluminum−silicon alloys in the presence of additives. An etched aluminium-silicon alloy, where the silicon particles protrude ∼1 μm from the metal surface, is used. We lubricate the sliding contact using an engine oil and track friction and wear of the alloy over 40 h.

2. EXPERIMENTAL SECTION

2.1. Wear Test. A near eutectic aluminium−silicon alloy in the as-cast condition was slid against the flat surface of a 1 mm diameter steel pin in a pin-on-disc (POD) instrument (displacement resolution ∼1 μm and load cell resolution ∼0.1 N, procured from DUCOM, Bangalore, India) under engine oil lubrication (see Supporting Information 1 for material details). All tests were run for 40 h (28.8 km). The experiments were done at two average contact pressures; (I) 12.7 MPa, which generated the UMW regime, and (II) 25.4 MPa, which generated the MW regime. The objective was to investigate the mechanical and chemical mechanisms of wear in the two regimes and to understand the long-term evolution of these mechanisms. The sliding test velocity was kept constant at 0.2 m/s during the test to emulate the piston ring velocity near the top dead centre of the engine. An oil flow rate was kept at 2 drops/min for all tests. The alloy samples were 160 mm in diameter and were ground and polished in the POD instrument to avoid additional hovelling of the polishing machine. The samples were etched with 10% NaOH solution for 60 sec, which was followed by washing in a 3% HNO_3 solution to remove the hydroxide layer. The average root mean square roughness of all samples was ∼0.25 μm and the average exposed height of silicon particles on the aluminium matrix was about 1μm. A diamond cutter (ISOMET 4000, BUEHLER) was used to cut the worn samples to the appropriate dimensions for subsequent analysis. All the data reported in this paper are done as function of sliding time, and at the same sliding velocity, which makes it easy to plot the data as a function of sliding distance.

2.2. Surface and Sub-Surface Study. 2D and 3D profiles of the wear tracks and of individual silicon particles were recorded using an optical surface profilometer (Wyko-MAR Precision System Inc), an environmental secondary electron microscope (Quanta 200, FEI), a FE-SEM (SIRION, FEG XL30, FEI), and an atomic force microscope (Innova, Veeco) respectively. Subsurface deformation in various places of the wear track was characterized by machining 30 × 8 × 8 μm trenches with a Focused Ion Beam (FIB) microscope (strata FIB 200xP FEI). A current of 2700 pA was used for the ion beam milling operation. Platinum was deposited next to the trench after milling using a current of 150 pA to protect the surface from beam damage. Ion beam polishing was performed after platinum deposition by using currents of 1000 pA and 350 pA, successively. Images were taken at an angle of 45° using beam currents of 11 pA and 70 pA the FIB. As the higher current of 70 pA may burn the substrate in places, the lower current of 11 pA was used as a reference of the higher current images to avoid the artifacts created by burning.

2.3. Lateral Force Microscopy (LFM). LFM experiments were performed using a pyramidal shaped Si_3N_4 tip of radius 30 nm in an AFM. A V-shaped cantilever with a spring constant of 0.57 N m^{-1} was used to measure the normal and lateral forces. All tips were cleaned in a UV chamber (Bioforce Nanosciences) for 20 min before use. The tests were conducted in a lubricated medium using the same lubricant as used for POD experiments described earlier. Lateral forces were recorded separately over an area of 5 μm × 5 μm of the polished aluminium matrix and an area of (5 μm × 5 μm) of the silicon particles. The lateral stiffness of the cantilever was measured using the finite element method in ABAQUS6.8 software. The dimensions of the cantilever were measured in the FE-SEM for cantilever stiffness estimation. The lateral force was measured according to the techniques mentioned by one of the authors in an earlier publication (25).

2.4. Chemical Analysis. The chemical composition of the worn discs and pins were studied in the Environmental Secondary Electron Microscope (Quanta 200, FEI). Surface-sensitive X-ray photo electron spectroscopy (XPS) was also used for chemical analysis of the worn surfaces coupled with MULTILAB 2000 instrument (Thermofisher Scientific). The spectrometer was equipped with a monochromatic Al$K\alpha$ (1486.6 eV) X-ray source and the beam size of the instrument was 4 mm × 4 mm. The C1s peak at 284.8 eV was used as a reference for the analysis. The observed spectra were deconvoluted using the

Gaussian-Lorenzian product function after background subtraction (26). The atomic concentration of the elements were calculated using atomic sensitivity factors published elsewhere (27).

2.4.1. *XPS Analysis.* Samples from the worn discs and pins were cut into 1 mm × 1 mm × 1 mm cubes with a diamond cutter. The worn samples were cleaned with ethanol for 5 min in an ultrasonicator and kept in a desiccator for 1 day. They were then kept in a UHV (ultra high vacuum) chamber for one more day to remove carbonaceous materials prior to the XPS analysis. A survey spectrum in the energy range of 0−1000 ev were taken from each sample. The major peaks that were observed on the survey spectrum were chosen for the high resolution scan. The scan was performed on Al2p, Fe2p, Ca2p, Si2p, C1s, O1s, Mo3d, S2p, P2p, and Zn2p peaks. Peak fitting was performed using the following procedure:

I. A least square fit was performed using the quadratic function on the raw XPS data to increase the signal-to-noise ratio (S/N). This smoothing procedure was performed several times without distorting the original peak.

II. The Shirley background correction (26) was performed on the smoothened data when the S/N ratio was high.

III. After the background correction, the peaks were deconvoluted using Fast Fourier Transformation using a software designed for fitting peaks on curves. The software used, calculates the peak position, area fraction of the individual peaks, peak intensity and total integrated area of the spectrum (see Supporting Information 2).

IV. Spin orbital splitting was done for elements where peaks overlapped. The separation energy of the split spin orbital and their relative ratios were maintained during curve fitting (see Supporting Information 3).

V. The carbon 1s peak with a binding energy of 284.8 eV was taken as a reference for all of the peaks. For all samples, the carbon 1s peaks were different because of carbon contamination, and the peak shift was calculated based on the peak value at 284.8 eV. All peak positions (binding energy) for a particular sample were corrected by the same peak shift as calculated above.

VI. Quantitative analysis was performed using a sensitivity factor for each element. If the intensity of the ith element is I_i and the corresponding sensitivity factor is S_i, then the atomic fraction is

$$N_i = \frac{{}^{I_i}/_{S_i}}{\sum_i {}^{I_i}/_{S_i}} \qquad \text{(A)}$$

The atomic fractions were converted into weight percent by using the atomic weight of the individual elements.

3. RESULTS

Our previous short duration sliding study (6) indicated the signatures which separate the ultra mild wear (UMW) regime from the mild wear (MW) regime. We have used the same partitioning criteria here. Figure 1a shows that at the lower contact pressure, the steady-state wear rate is 5.74×10^{-19} m^3/s, an equivalent normal ball displacement rate is of the order of 0.5 nm/s. This we designate as UMW regime. When the contact pressure is in the MW regime, there is a rapid wear rate of 8.7×10^{-18} m^3/s until about 15 h, beyond the initial run-in for 2 h. This rate is very similar to what was earlier characterized as oxidative mild wear (6). The wear

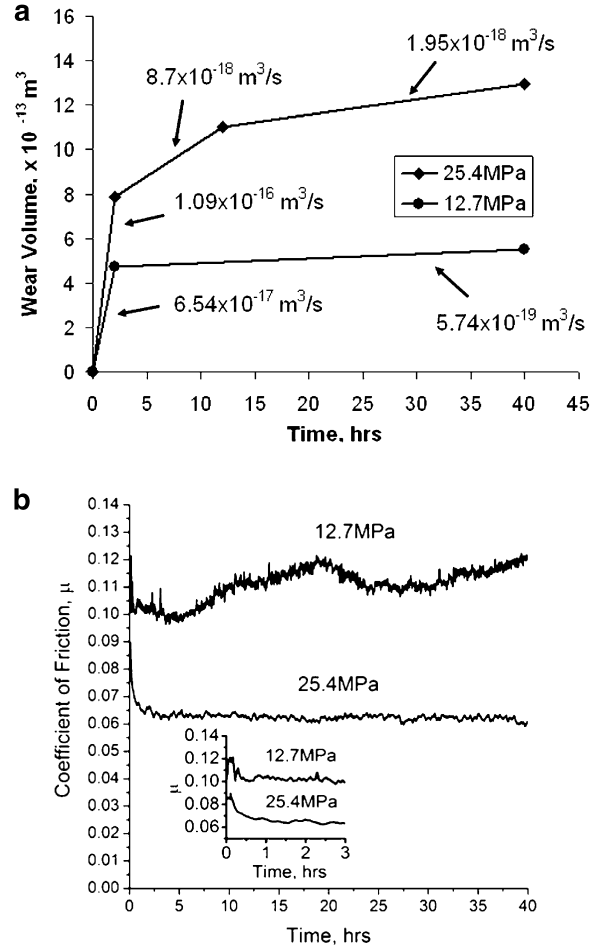

FIGURE 1. (a) Wear volume plotted against sliding time at different pressures. Wear depth measured by the optical profilometer at different sliding times. (b) Coefficient of friction plotted as a function of sliding time. The inset shows the variation of coefficient of friction during the first 3 h.

rate decreases after 17 h to a steady state value (1.95×10^{-18} m^3/s), which is 3.3 times that of the steady state UMW wear rate.

Figure 1b shows the coefficient of friction to increase from about 0.1 to 0.12 in 40 h, when the contact pressure is 12.7 MPa. Doubling the pressure shows a decrease from 0.09 to about 0.062 in 5 h and a very gradual decrease in the period between 5 and 40 h.

3.1. Ultra-Mild Wear Regime. Figure 2a confirms that the silicon columns stand proud of the aluminum matrix during the UMW regime. The average volume loss over the wear track shown in Figure 1a was estimated from the profilometric data recorded such as in Figure 2a.

The silicon particle height on the unslid surface is described by a Gaussian distribution, and in the first 2 h, the tips of the taller particles are worn and fractured leading to a 600 nm reduction of the average height. This corresponds to a steep rise in the wear volume. Figure 3 shows the abrasion marks on top of a silicon particle following the 2 h of sliding in the UMW regime. The FIB cross section of the sample worn in this time period shows intense plastic deformation of the matrix near the silicon−matrix interface and failure at some locations, but does not show any

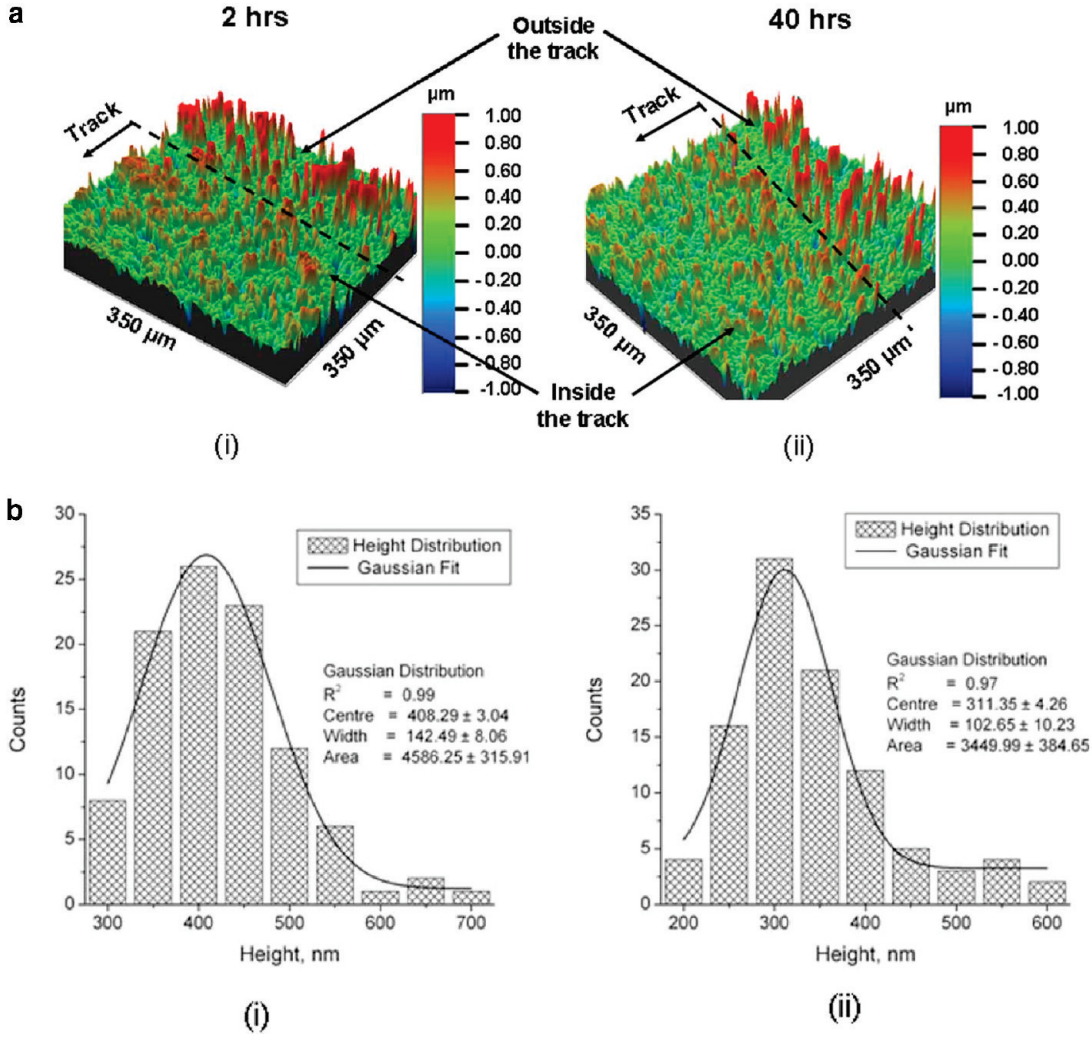

FIGURE 2. (a) 3D topography of the worn surface slid for (i) 2 h and (ii) 40 h at a contact pressure 12.7 MPa (UMW regime). Green color represents the average height of the aluminium matrix. Deep red colour represents the unworn silicon particles outside the tracks whereas light red colour shows the worn out silicon particles within the track. (b) The height distribution of worn out silicon particles after (i) 2 h and (ii) 40 h of sliding. The Gaussian curve fit to the distribution shows that the average height (centre) of silicon particles is ~400 nm after 2 h and ~300 nm after 40 h of running.

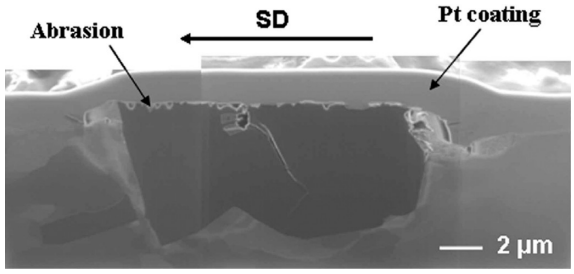

FIGURE 3. FIB sectioned subsurface of the UMW regime shows deformation around the silicon particle after 2 h of running. SD - Sliding direction.

continuous decohesion of the particle−matrix boundary or any sliding of the particle in the matrix by shearing at the interface. We surmise that the high volumetric wear of the track in the first 2 h is not associated with any significant sinking of the particle, but primarily reflect the wear of the Si particles themselves. The first 2 h of high wear is followed by a slow reduction of 100 nm of particle height in the next 38 h (Figure 2). This corresponds to a volumetric loss of only one-sixth of that in the first 2 h. The following are some of the qualitative observations of the attrition process during the 40 h of UMW.

(1) The pin surface undergoes changes due to contact. Initially, the pin is severely abraded by the silicon particles, but with time, the pin becomes smooth, as seen in images a and b in Figure 4.

(2)Iron is found at the edge of the silicon particle on the disc suggesting that the silicon particles scrape/abrade the softer pin (supporting information (4)).

(3) The silicon particles on the disc chip off or fracture with time and get embedded into the soft pin. The line profile of the surface shown in Figure 4c suggests that although the abrasion marks are absent on the pin after 40 h of sliding, the pin carries 100−200 nm high protrusions (shown by arrows), which may be embedded silicon particles. This is supported by the XPS data (Table 1), which shows the presence of silicon on the pin surfaces in the UMW but not in the MW regime. XPS analysis of these fragments embedded on the pin indicate that these fragments are made of $Si(OH)_4$ (see Supporting Information 5).

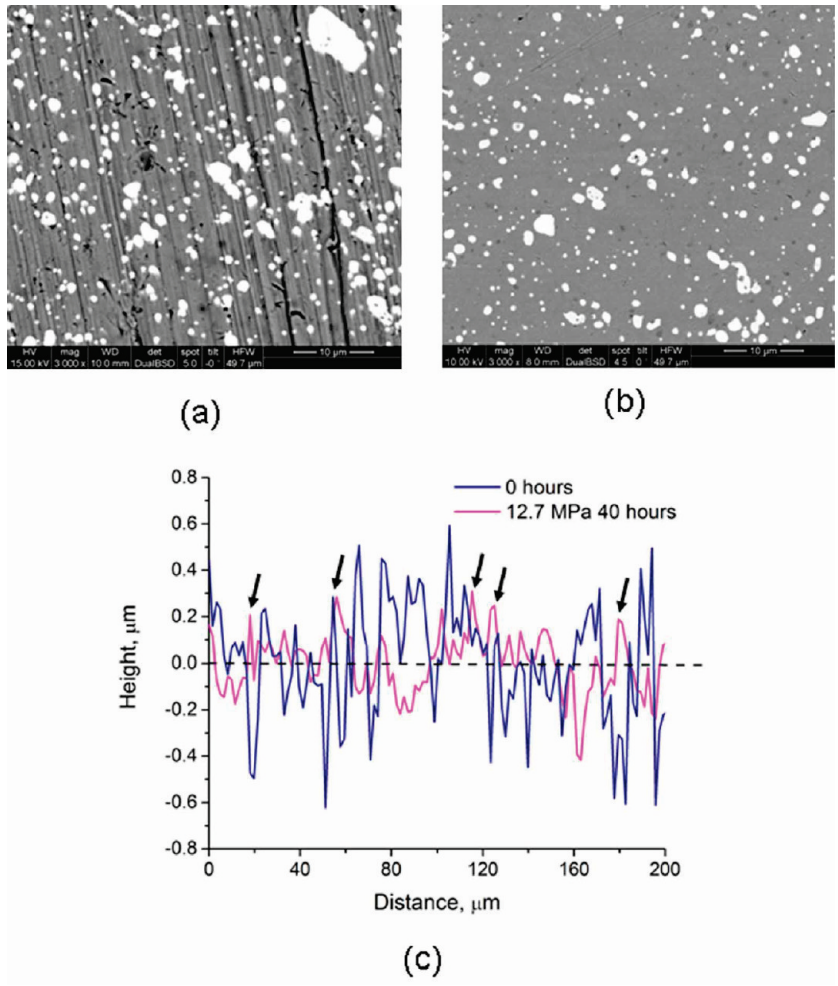

FIGURE 4. SEM micrograph of (a) unslid pin and (b) pin slid for 40 h at 12.7 MPa contact pressure, showing the smoothening of the surface with time. (c) Corresponding line profiles across the pin surface.

Table 1. XPS Elemental Analysis (accuracy of the results is estimated to be better than 6%)

	elemental composition in wt %			
elements	disc, 12.7 MPa, 40 h	disc, 25.4 MPa, 40 h	pin, 12.7 MPa, 40 h	pin, 25.4 MPa, 40 h
C	34.15	39.27	58.93 (0.85)[a]	57.61
O	39.11	36.91	28.79	26.83
Al	10.99 (86.24)[a]	6.46	0	0
Si	5.04 (12.26)[a]	2.31	1.59 (0.24)[a]	0.01
Fe	7.30	9.45	8.18 (82)[a]	8.86
Mo	0.70 (0)[a]	2.14	0.54 (5.01)[a]	2.39
S	1.06	1.48	0.8	2.41
P	1.19 (0)[a]	1.45	0.78 (0.02)[a]	1.12
Zn	0.47 (0.09)[a]	0.55	0.38	0.76
Cr			0 (3.76)[a]	0
V			0 (1.83)[a]	0
Mn			0 (0.23)[a]	0
W			0 (6)[a]	0

[a] Numbers in parentheses give the wt % in the unslid disc and pin (see the Supporting Information, 1).

(4) Another damage mode is the abrasion of the silicon particles on the disc by the silicon fragments embedded in the pin. The LFM images (see Supporting Information 6) of the particle give an average attrition of 30 nm in 38 h. The total reduction of the silicon protrusion in 38 h being 100 nm, we suggest that there is a 70 nm reduction of the protrusion by sinking in this time and this happens mainly at large sliding times (no sinking occurs in the first 2 h).

In previous publications (4−6), we have shown that if the matrix at the root of a silicon particle deforms plastically, the particle sinks into the matrix. Figure 5 shows that after 40 h of sliding, decohesion, voids, and continuous cracks have occurred around the particles at the silicon-matrix interface. Comparing Figures 3 and 5, it is clear that this continuous failure of the interface happens at high sliding times approaching 40 h and that particle sinking is a major cause for volumetric loss in the 2−38 h period. The most likely explanation for particle sinking at low contact pressure and high sliding time may be high cycle fatigue, weakening a region around the root of the silicon particle. The reduction in the quantity of Si and Al on the disc surface (Table 1) after sliding in the UMW regime, and the corresponding appearance of Zn, P, S, and Mo when they were not there on the as-received material (see Supporting Information 1), suggests that the spectrometer detected the presence of a third body film on the matrix. The elemental composition of the pin surface shows a reduction in the quantities of Fe and Mo,

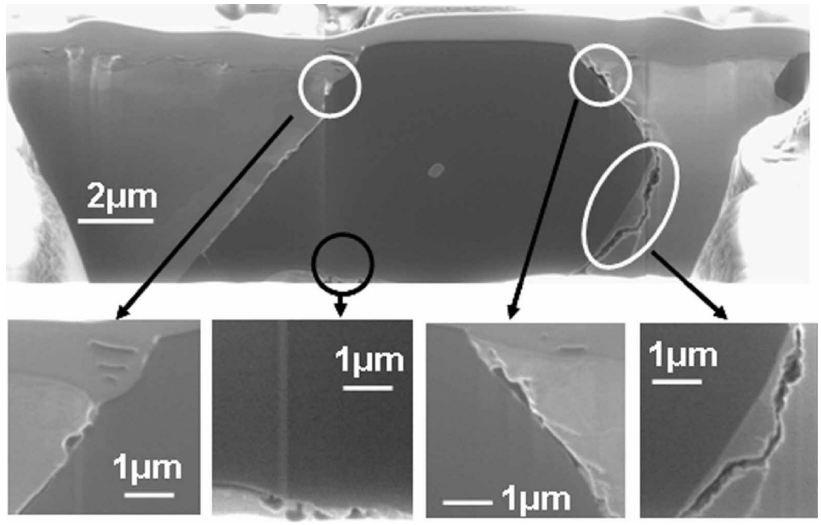

FIGURE 5. FIB sectioned subsurface in the UMW regime showing interfacial delamination around the silicon particles when the surface is slid for 40 h. SD is perpendicular to the plane of the paper.

Table 2. Summary of Oxygen 2p Peaks[a]

sample	peak	area (%)	species	BO/NBO,α	theoretical value of α, (Martin 99)	phosphate type (Martin 99)
Al−Si disc, 12.7 MPa, 40 h	529.9	16.23	oxide	0.45	$0.41 < \alpha < 0.47$	$\alpha \approx 0.47$, $Zn_{20}P_{38}O_{115}$
	531.7	21.91	NBO			
	532.81	38.34	C−OH			
	533.41	9.83	BO			
	534.31	13.68	C−O			
Al−Si disc, 25.4 MPa, 40 h	530.00	29.32	oxide	0.29	$0.19 < \alpha < 0.36$	mixture of $Zn_2P_2O_7$ ($\alpha \approx 0.19$) & $Zn_4P_6O_{19}$ ($\alpha \approx 0.36$)
	531.70	15.63	NBO			
	532.84	31.05	C−OH			
	533.4	4.52	BO			
	534.43	19.48	C−O			
steel pin, 12.7 MPa, 40 h	530.01	26.95	oxide	0.21	$0.19 < \alpha < 0.36$	$\alpha \approx 0.19$, $Zn_2P_2O_7$ (pyrophosphate)
	531.71	27.18	NBO			
	532.61	30.23	C−OH			
	533.38	5.65	BO			
	534.44	9.99	C−O			
steel pin, 25.4 MPa, 40 h	530	31.56	oxide	0.36	$\alpha = 0.36$	$Zn_4P_6O_{19}$
	531.7	22.73	NBO			
	532.6	27.03	C−OH			
	533.4	8.10	BO			
	534.4	10.58	C−O			

[a] The peaks were deconvoluted into five peaks based on the results present in ref 29. The estimated error in the binding energy is within ±0.2 eV and area fraction within 8%.

an enhancement in P, disappearance of Cr, V, Mn, and W, and appearance of Si and S. The latter suggests that the pin surface is covered with a tribofilm. Whether the silicon detected is embedded silicon or silicon in the tribofilm is not clear at this stage.

The O1s spectra (28, 29) (see Supporting Information 7) indicates the presence of iron and zinc oxide (530.2 ± 0.1 eV), polyphosphate, sulphate, carbonate, and hydroxide in non-bridging oxygen (531.8 ± 0.1 eV) and phosphates (linked) in bridging oxygen (BO - 533.4 eV). The Fe2p and P2p spectra (see Supporting Information 8) indicate the presence of zinc orthophosphate ($Zn_3(PO_4)_2$ −132.9 eV), and iron phosphate ($FePO_4$ −713.8 eV). There are traces of organo sulphur, sulphides, and sulphates on the pin surface. The C1s spectrum indicates the presence of substantial amount of carbonyl functions (C═O) in the tribofilm. Table 2 shows the O2p spectra summary to indicate the presence of zinc pyrophosphate on the pin. The table also shows a low ratio of BO/NBO for the pin indicating short linkages of the phosphates. The disc shows an almost identical O1s spectrum, except that it has a higher BO/NBO ratio (Table 2), indicating the presence of longer-chain phosphates.

3.2. Mild Wear Regime. Figure 6 shows that most of the protruding silicon particles disappear after 2 h of sliding in the MW regime, whereas Figure 7 shows that a conformal (to the spherical pin geometry) plastic groove develops, the groove depth increases in time (see pile up in

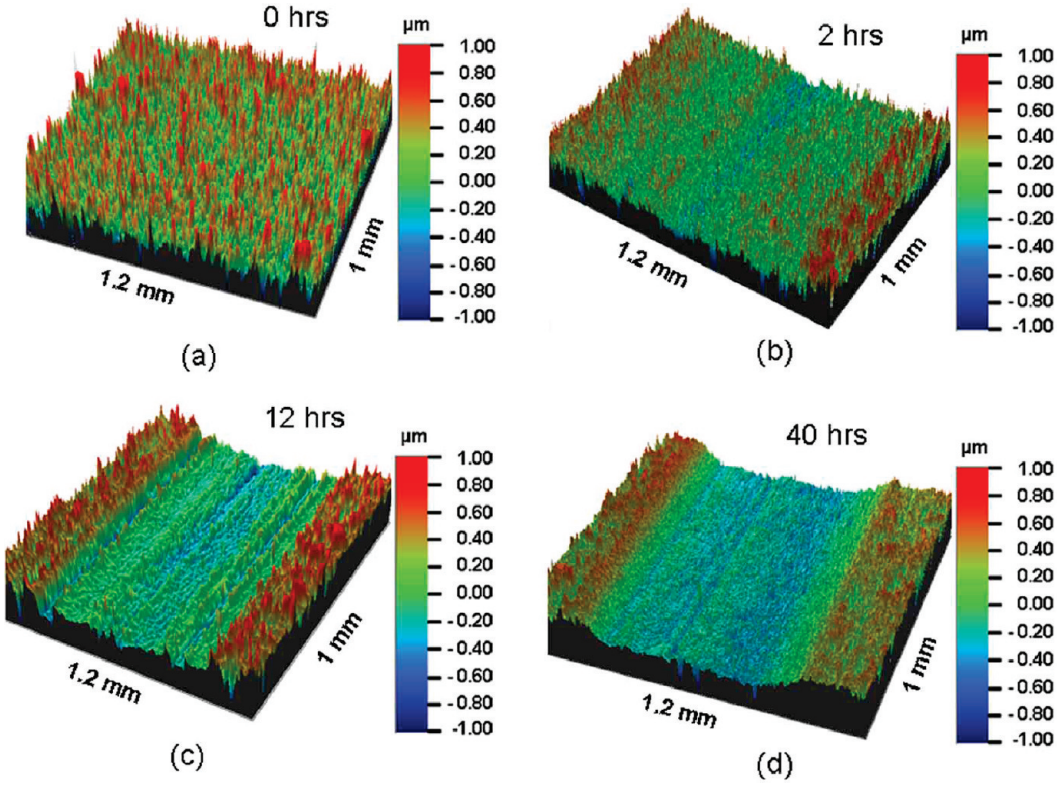

FIGURE 6. 3D topography of worn surfaces slid at 24.5 MPa for (a) 0, (b) 2, (c) 12, and (d) 40 h. The dark red color represents the highest part of the surface and the dark blue represents the deepest part of the surface.

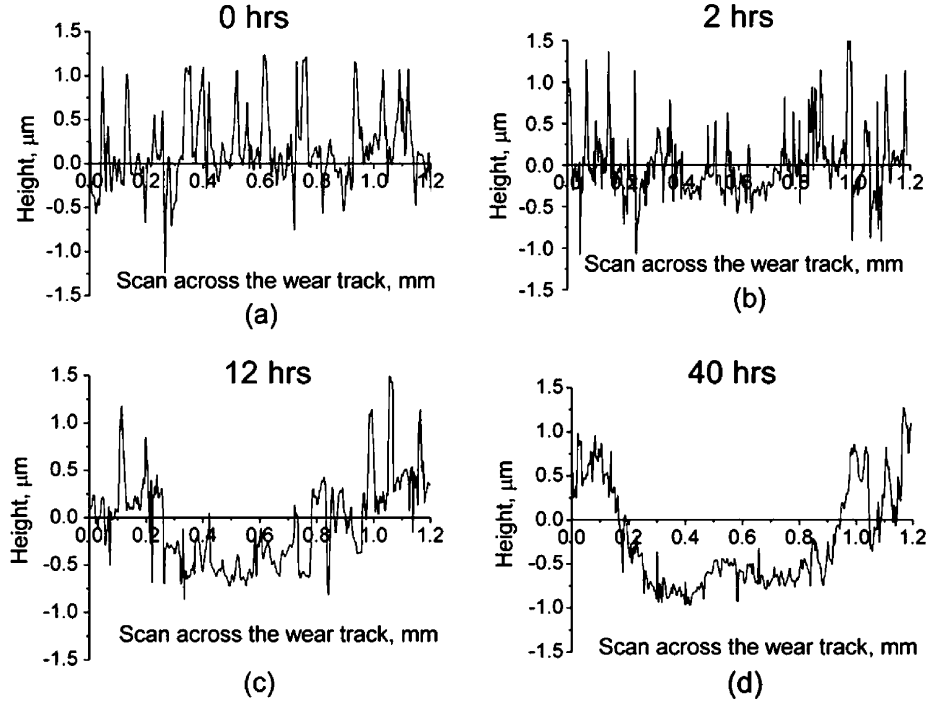

FIGURE 7. 2D profiles of the wear tracks formed at 24.5 MPa for different sliding times: (a) 0, (b) 2, (c) 12 h, and (d) 40 h.

panels c and d in Figure 7). The subsurface is severely damaged in plasticity which promotes the formation of subgrains near the surface (Figure 8). Table 1 shows a significant enhancement of Mo, S, and Zn on the pin surface over what was detected in the UMW regime. Further, unlike in the case of UMW regime, no Si is detected on the pin surface. The XPS results (Table 2) show polyphosphate on the pin surface, and a mixture of polyphosphate and orthophosphate on the disc surface.

The minor chemical difference between the UMW and MW regimes is that the higher pressure reduces the quantity of hydrocarbon (oil) and increases the presence of sulphides. The major difference is that higher pressure in the MW regime generates greater quantities of MoS_2 on the pin

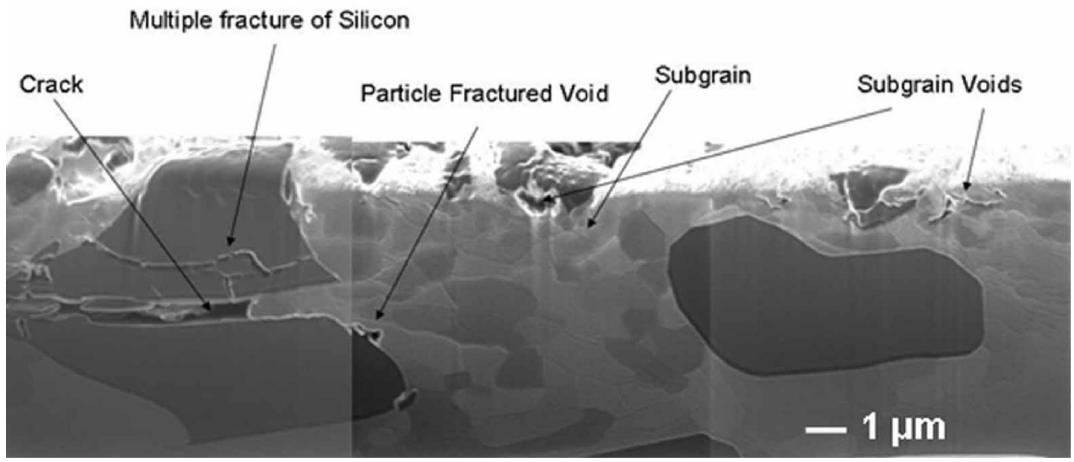

FIGURE 8. FIB sectioned subsurface of the disc slid for 40 h in the MW regime showing plastic deformation in the near-surface region. SD is perpendicular to the plane of paper.

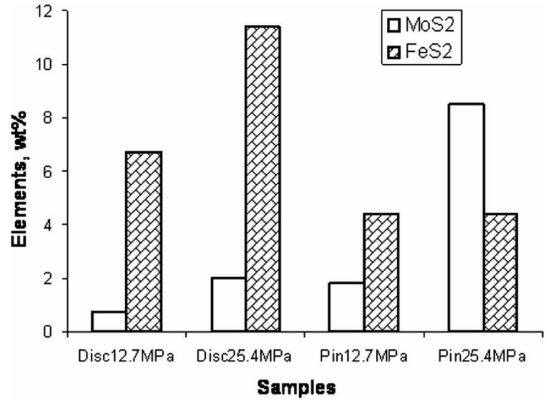

FIGURE 9. Bar chart of FeS_2 and MoS_2 elements for pin and disc surfaces slid for 40 h. The weight percent of the elements were calculated from the XPS analysis without considering the oxygen and carbon peak.

(Figure 9) and a greater quantity of FeS_2 on the disc than what is achieved in the UMW regime. MoS_2 is a strong antifriction agent while FeS_2 is an amorphous material (30), which protects the iron from oxidation, and is thus an antiwear agent (31). Otherwise, the XPS data obtained from both the pin and disc surfaces show the formation of glassy polyphosphates as well as some polymerized phosphate.

4. DISCUSSION

The polyphosphates, FeS_2, $FePO_4$ detected on the pin surface in the UMW regime suggests that even at this very low contact pressure, the ZDDP additive decomposes and forms a tribofilm. We believe that the nascent iron (8, 9), generated by abrasion of the pin by the protruding silicon particles catalyses the decomposition. There is a cataionic exchange that replaces Zn in ZDDP with iron to give rise to a more unstable compound, which decomposes readily to yield a host of reaction products. These reaction products, however, do not participate in yielding low friction in the UMW regime. We believe that this happens because the reaction products migrate to the valleys between the silicon columns, and the only contact at the low sliding time is lubricated ploughing/abrasion of iron by sharp silicon particles, and the abrasion of the silicon particle by the $Si(OH)_4$ embedded on the soft pin (see schematic, Figure 10). Lateral force microscopy of the protruding silicon particle in an oil medium with a Si_3N_4 probe gave a coefficient of friction of 0.11−0.17 (in the normal load range of 30−70 nN). The corresponding coefficient of friction for the steel probe is about 0.09. The coefficient of friction recorded at the commencement of sliding in the UMW regime is 0.11−0.12 (Figure 1b). With increasing sliding time, the silicon particle height is distributed more uniformly (Figure 2a), giving rise to an increase in contact area and a consequent increase in the friction force (Figure 1b) at 12.7 MPa. Although this (μ increasing with sliding time) happens for about 30 h of sliding (Figure 11), the silicon particles wear out gradually. In the process, a new dissipation mechanism which results in a reduction of coefficient of friction with sliding time is ushered in. We believe that the silicon particles wear out with sliding, the tribofilms on the pin and the disc come into contact with each other, replacing gradually the predominance of the high friction abrading contact by low friction contacts where the tribofilm is sheared. As more such patches of "tribofilm contact" occur, the area average, of the abrasion friction by the silicon particle on the pin, and the tribofilm friction, would decrease. Figure 11 shows this phenomenon for different contact pressures. At the highest test pressure of 19 MPa within the UMW regime, the friction coefficient after 140 h of sliding declines to 0.06, a value characteristic of steady state MW friction.

The major difference between the reaction products generated in the UMW and MW regimes is the presence of a large amount of MoS_2 in the latter, which is a strong antifriction agent. As the pressure is increased from the UMW to the MW regime, the molybdenum in the steel replaces the Zn in ZDDP through a cationic exchange (8, 30, 32). This exchange yields a relatively more unstable compound, and further decomposition and recombination gives MoS_2 (33, 34). The contact pressure in MW regime is more than that corresponding to the elastic shakedown limit (6) of the aluminium−silicon alloy. Formation of subgrains (Figure 8) in the subsurface testifies to the state of plasticity. At the commencement of sliding the protruding silicon

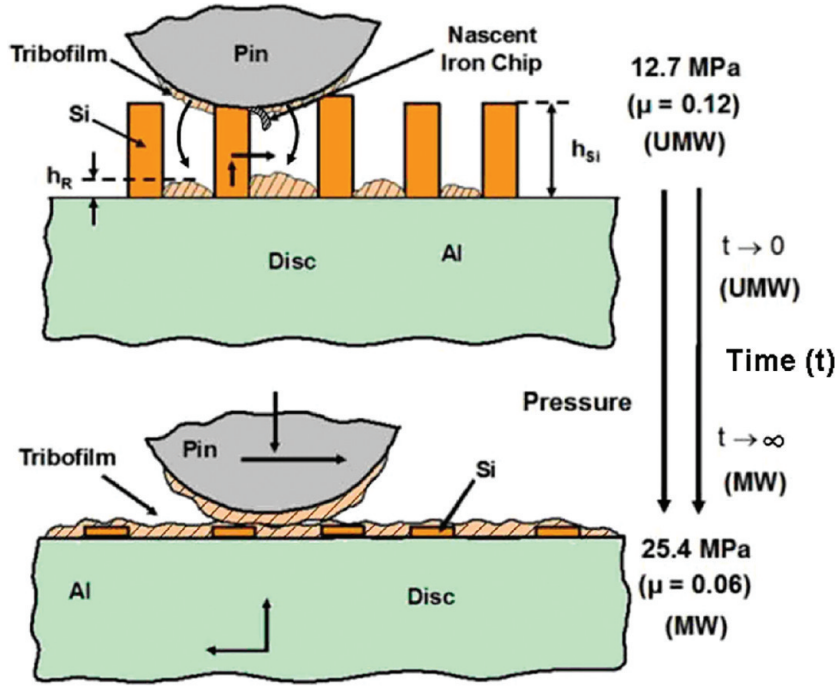

FIGURE 10. Schematic diagram (not to scale) representing the interaction between aluminium−silicon alloy, steel counterface, and tribofilm formed during sliding in the UMW and MW regimes. The schematic is not to scale.

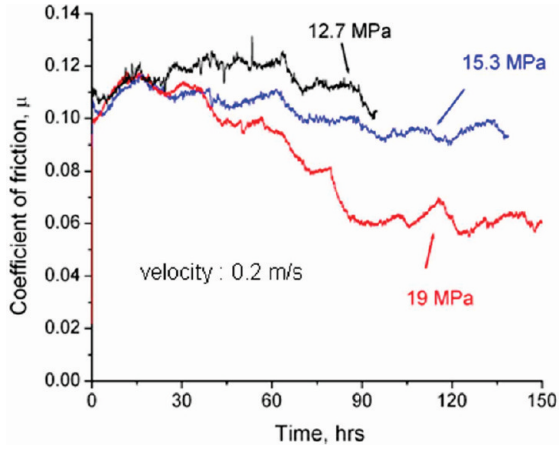

FIGURE 11. Coefficient of friction plotted as a function of time at different contact pressures.

abrades the pin yielding a friction coefficient of about 0.09. The silicon particles in the first 2 h break and fracture, reducing their height as they sink into the plastic matrix. After 2 h of sliding, a near conformal smooth contact is established between the pin and the substrate (Figure 7b). At such times, the tribofilm with antifriction compounds of MoS_2, polyphosphate glass, FeS_2 etc. (8, 9, 29, 31) become operative over the whole contact area to establish a coefficient of friction of 0.06, which is invariant with time.

One of the most interesting findings of this work is that although there are two distinct stages of lubricated wear in Al−Si alloys in the low pressure range, the distinction being defined by the contact pressure, the friction is totally determined by the kinetics of the contact condition. The morphology of the surface of this two-phase alloy is such that the contact condition undergoes profound changes with sliding time, so much so that at a given contact pressure in the UMW regime, there is a sliding time after which the coefficient of friction is the same as that achieved at a higher pressure in the mild wear regime, albeit after a shorter sliding time. This sliding time when the friction coefficients of the two regimes converge depends on the contact pressures operating in both regimes. For example, at a low pressure such as 10−12 MPa in the UMW regime, it may take more than 500 h for this convergence to occur, but increasing the pressure to 19 MPa in the UMW regime causes the sliding time required for convergence to decrease to 140 h to approach the coefficient of friction corresponding to the MW regime. The same coefficient of friction is also achieved at higher contact pressures of 25−27 MPa, but after a much shorter time of only 1/5−2 h of sliding time when the experiment is done in the MW regime. Until the onset of the severe wear regime (50−70 MPa) (35), the present work indicates that it is always possible to obtain a low friction regime for these alloys, as long as adequate sliding time is permitted. What the designer, however, has to be careful about is that, although a low friction is attainable at any pressure, in this pressure range lie two regimes of wear; and the MW rate is about three times that of the corresponding UMW rate. Taking these facts into consideration, it seems safe to limit the running-in pressure to the higher limit of the UMW regime.

5. CONCLUSIONS

An aluminium−silicon alloy disc was slid against a steel pin under lubrication at a low velocity (0.2 m/s) and two pressures: 12.7 MPa, characteristic of ultra-mild wear (UMW),

and 25.4 MPa, characteristic of mild wear (MW). The following conclusions can be made:

(I) There are three processes that simultaneously control friction almost identically in the two regimes of wear:

(i) Abrasion of the steel counterface by silicon.

(ii) Wear of silicon and sinking of silicon into the matrix.

(iii) Generation of nascent steel chips by abrasion, which aid to decompose the additives in the lubricant to yield friction modifying chemical products.

The relative importance of the three processes at any given sliding time is dependent on the average contact pressure. The sliding time required to achieve an exclusive chemically induced friction coefficient may be very long in the ultra mild wear regime, whereas it may be quite short in the mild wear regime. At very long sliding times, the steady-state friction coefficients of the two regimes converge to similar values of 0.06.

(II) Whereas the activities occurring at the sliding interface in different regimes may generically be the same, the stress state of the material in the slid subsurfaces may be qualitatively different in yielding different orders of wear. It is, therefore, acceptable to delineate wear regimes by characteristic magnitudes of wear and corresponding pressure ranges (at constant velocity).

Acknowledgment. The authors are grateful to Mr. Sadhu Rajasekhar, Mrs. Savitha, and Mr. Sham Sundar for their cooperation in the experimental work. The authors from the IISc are also thankful to the General Motors (R &D), Warren, MI, for the financial support to conduct this research.

Supporting Information Available: Supporting information 1 gives the material details; supporting information 2 and 3 show examples of deconvolution of different XPS spectra; supporting information 4 shows that iron is present at the edge of silicon particles; supporting information 5 shows the deconvoluted XPS spectra of the transferred silicon on the steel counterface; supporting information 6 shows the AFM topography of the abraded silicon particles; supporting information 7 shows the deconvoluted XPS spectra of the oxygen 2p peaks; supporting information 8 shows the deconvoluted XPS spectra of the transferred iron and phosphrous on the disc in UMW regime. This material is available free of charge via the Internet at http://pubs.acs.org.

REFERENCES AND NOTES

(1) Dienwiebel, M.; Pohlmann, K.; Scherge, M. *Tribol. Int.* **2007**, *40*, 1597–1602.
(2) Riahi, A. R.; Perry, T.; Alpas, A. T. *Mater. Sci. Eng., A* **2003**, *343*, 76–81.
(3) Das, S.; Perry, T.; Biswas, S. K. *Tribol. Lett.* **2006**, *21*, 193–204.
(4) Mahato, A.; Sachdev, A. K.; Biswas, S. K. *Wear* **2008**, *265*, 849–855.
(5) Mahato, A.; Xia, S.; Perry, T.; Sachdev, A. K.; Biswas, S. K. *Tribol. Int.* **2010**, *43*, 381–387.
(6) Mahato, A.; Perry, T. A.; Jayaram, V.; Biswas, S. K. *Wear* **2010**, *268*, 1080–1090.
(7) Dey, S. K.; Perry, T. A.; Alpas, A. T. *Wear* **2009**, *267*, 515–524.
(8) Spikes, H. *Tribol. Lett.* **2004**, *17*, 469–489.
(9) Nicholls, M. A.; Do, T.; Norton, P. R.; Kasrai, M.; Bancroft, G. M. *Tribol Int.* **2005**, *38*, 15–39.
(10) Martin, J. M. *Tribol. Lett.* **1999**, *6*, 1–8.
(11) Chen, M.; Meng-Burany, X.; Perry, T. A.; Alpas, A. T. *Acta Mater.* **2008**, *56*, 5605–5616.
(12) Nicholls, M. A.; Norton, P. R.; Bancroft, G. M.; Kasrai, M.; Stasio G., De; Wiese, L. M. *Tribol. Lett.* **2005**, *18*, 261–278.
(13) Pereira, G.; Lanchenwitzer, A.; Nicholls, M. A.; Kasrai, M.; Norton, P. R.; Stasio, G. De *Tribol.Lett.* **2005**, *18*, 411–427.
(14) Hongbing, Ji.; Nicholls, M. A.; Norton, P. R.; Kasrai, M.; Capehart, T. W.; Perry, T. A.; Cheng, Y. *Wear* **2005**, *258*, 789–799.
(15) Das, S.; Biswas, S. K. *Tribol. Lett.* **2004**, *17*, 623–628.
(16) Timmermans, G.; Froyen, L. *Wear* **1999**, *231*, 77–88.
(17) Wan, Y.; Cao, L.; Xue, Q. *Tribol. Int.* **1997**, *30*, 767–772.
(18) Nautiyal, P. C.; Schey, J. A. *Trans. ASME, J. Tribol.* **1990**, *112*, 282–287.
(19) Tseregounis, S. I. *Tribol. Trans.* **1996**, *39*, 1–12.
(20) Sargent, L. B.; Milz, W. C.; Atkinson, R. E. *Lubr. Eng.* **1983**, *39*, 706–711.
(21) Schey, J. A.; Nautiyal, P. C. *Wear* **1991**, *146*, 37–51.
(22) Kawamura, M.; Fujita, K. *Wear* **1983**, *89*, 99–105.
(23) Wan, Y.; Xue, Q. *Tribol. Int.* **1995**, *28*, 553–556.
(24) Wan, Y.; Xue, Q. *Tribol. Lett.* **1996**, *2*, 37–45.
(25) Devaprakasam, D.; Khatri, O. P.; Shankar, N.; Biswas, S. K. *Tribol. Int.* **2005**, *38*, 1022–1034.
(26) Seah, M. P. *Practical Surface Analysis*, 2nd ed.; Wiley: Chichester, U.K., 1983; chapter 3.
(27) Crankovic, G. M., *ASM Handbook, Vol. 10: Material Characterization*, fifth ed.; ASM International: Materials Park, OH, 1998.
(28) Heuberger, R.; Rossi, A.; Spencer, N. D. *Tribol. Lett.* **2007**, *25*, 185–196.
(29) Morina, A.; Neville, A.; Priest, M.; Green, J. H. *Tribol. Int.* **2006**, *39*, 1545–1557.
(30) Ito, K.; Martin, J. M.; Minfrey, C.; Kato, K. *Tribol. Int.* **2006**, *39*, 1538–1544.
(31) Morina, A.; Neville, A.; Priest, M.; Green, J. H. *Tribol. Lett.* **2006**, *24*, 243–256.
(32) Bai, M.; Zhang, X.; Qi, S. *Wear* **1993**, *169*, 181–187.
(33) Yamamoto, Y.; Gondo, S. *Tribol. Trans.* **1989**, *32*, 251–257.
(34) Martin, J. M.; Mogne Th. Le, Grossiord, C.; Palermo, Th. *Tribol. Lett.* **1996**, *2*, 313–326.
(35) Das, S.; Varalakshmi, K.; Jayaram, V.; Biswas, S. K. *Trans. ASME, J. Tribol.* **2007**, *129*, 942–951.

AM100550M